Journal of Nuclear Materials 511 (2018) 64–74

Contents lists available at ScienceDirect

Journal of Nuclear Materials

journal homepage: www.elsevier.com/locate/jnucmat

Defect structures and statistics in overlapping cascade damage in fusion-relevant bcc metals

A.E. Sand*, J. Byggmästar, A. Zitting, K. Nordlund

Department of Physics, University of Helsinki, P.O. Box 43, FI-00014, Helsinki, Finland

ARTICLE INFO

Article history:
Received 10 April 2018
Received in revised form
22 August 2018
Accepted 27 August 2018
Available online 31 August 2018

Keywords:
Tungsten
Iron
Radiation damage
Lattice defects
Molecular dynamics

ABSTRACT

Most experimental work on radiation damage is performed to fairly high doses, where cascade overlap effects come into play, yet atomistic simulations of the primary radiation damage have mainly been performed in initially perfect lattice. Here, we investigate the primary damage produced by energetic ion or neutron impacts in bcc Fe and W. We model irradiation effects at high fluence through atomistic simulations of cascades in pre-damaged systems. The effects of overlap provide new insights into the processes governing the formation under irradiation of extended defects. We find that cascade overlap leads to an increase in the numbers of large clusters in Fe, while in W such an effect is not seen. A significant shift in the morphology of the primary damage is also observed, including the formation of complex defect structures that have not been previously reported in the literature. These defects are highly self-immobilized, shifting the damage away from the predominance of mobile $1/2\langle 111\rangle$ loops towards more immobile initial configurations. In Fe, where cascade collapse is extremely rare in molecular dynamics simulations of individual cascades, we observe the formation of vacancy-type dislocation loops from cascade collapse as a result of cascade overlap.

1. Introduction

Macroscopic effects of radiation damage in materials, such as swelling and embrittlement, result from the gradual accumulation of atomic scale primary damage from particle impacts, combined with the simultaneous thermal evolution of the microstructure. The concurrent creation of new defects and evolution of existing defects leads to differences in the long term damage accumulation depending on factors such as irradiation temperature, dose and dose rate [1]. Radiation damage formation on the picosecond time scale from individual energetic particle impacts is fairly well understood, from a large body of molecular dynamics work. However, practical applications require predictions of damage over much longer time scales, and to doses where it is clear that every region of the material has been hit multiple times.

In a nuclear environment, such as in fission and future fusion reactors, the reactor walls will be subject to long term radiation exposure, with the energetic neutron irradiation eventually leading to the degradation of mechanical and thermal properties of the materials. During the life time of the reactor component, an average radiation dose ranging from tens of dpa up to 200 dpa will be reached in various reactor types [2]. Ion irradiation experiments, useful as a proxy for studying neutron irradiation effects, are also often carried out to a dpa well above the limit where overlap effects can be expected to occur.

Although both α-Fe and W have the bcc crystal structure, their response to energetic ion irradiation differs markedly, with visible (by means of TEM) defects appearing immediately upon irradiation in W, but only after some time in Fe. Experimental evidence points to an effect of cascade overlap on the formation of dislocation loops in both neutron- [3] and self-ion [4] irradiated Fe. This conjecture is based on two qualitatively different observations: the negative curvature of differential dose curves from resistivity measurements in neutron-irradiated Fe reported by Dunlop *et al.* [3], and the appearance of TEM-visible defects in self-ion irradiated Fe only after a threshold dose level, together with a subsequent non-linear increase in visible defects demonstrated by Robertson *et al.* [4]. Later careful investigation by Schäublin *et al.* of low-dose self-ion irradiation has found visible defects at a much lower fluence [5]. However, the samples in this later work were irradiated with 150 keV Fe ions, while the work by Robertson *et al.* used 50 and 100 keV Fe ions. Both simulation and experiment indicate that

* Corresponding author.
E-mail address: andrea.sand@helsinki.fi (A.E. Sand).

https://doi.org/10.1016/j.jnucmat.2018.08.049
0022-3115/

more, and larger, defects are produced from higher energy cascades [4,6,7], with this effect extending beyond the point where cascades begin to split into separate subcascade regions (which in Fe is around 20–30 keV [8]). Hence these observations are not necessarily in contradiction to each other.

The overlap effect conjectured by Dunlop, and later supported by Robertson, concerns the collapse of vacancy-rich areas into vacancy-type loops, also referred to as cascade collapse [9,10]. However, the nature of the black dots observed by transmission electron microscopy (TEM) of irradiated Fe is in most cases not clear. Due to the difficulty of determining the nature of the very small dislocation loops, very few studies have done this explicitly. Robertson *et al.* assume the loops they observe in Fe are of vacancy type [4], based on previous irradiations with heavy ions. Previous work by these authors [11] used the direction of the black-white streaking of the loop image, and comparison to simulated images, to determine that the loops they observed in Ni and Ni alloys irradiated with heavy ions were all of vacancy type. It should be noted, however, that this method only works for fairly large loops, and is not in general possible with the small loops observed in neutron- and self-ion irradiated Fe at low doses and temperatures. Masters [12] determined the nature of observed loops based on the change in their apparent size when passing through an absorption band, and found only interstitial-type loops. However, the results were from irradiations performed at 550 °C, at which temperature vacancy-type loops can be expected to evaporate, based on rate theory arguments [9,13]. Based on the same rate theory argument, in the work by Jenkins *et al.* [9], loops are also assumed to be of vacancy type, due to the low dose and proximity of the surface. The rapid evaporation of vacancy loops in Fe at elevated temperatures has also recently been predicted theoretically using a hybrid mean field approach coupled with a real space model of irradiation induced defects [14]. In W, on the other hand, loops are generally larger, and a determination of the vacancy or interstitial nature has revealed the presence of both morphologies among the visible loops in self-ion irradiated W and W–5Re [15].

In thermally activated clustering of individual vacancies, 3-dimensional voids would be expected to form, rather than loops, due to the lower formation energy of voids in both Fe and W [16]. However, once vacancy-type loops are formed, they may migrate similarly to interstitial-type loops [17], facilitating the growth of loops through coalescence [18]. Attempts at modelling the microstructural evolution of materials under irradiation have mainly focussed on the thermal evolution and interactions of the defects [19–24]. Generally, it is assumed that the primary damage created from particle impacts is independent of the evolving state of the material. However, as the fluence increases, the chances of cascades occurring on top of existing defects also increases.

The damage production due to collision cascades, initiated by impacts of energetic neutrons or ions, takes place on time scales too short to be directly observed with experimental methods. Atomistic simulations, such as molecular dynamics (MD), can instead be used to provide information about the nature of the primary damage produced by cascade events. Although the primary damage caused by collision cascades has been extensively studied in MD simulations (see, e.g. [25–27]), most cascade simulations have taken a perfect lattice as a starting point. While simulations indicate that the effect of temperature on the primary damage is indeed negligible under most circumstances, the few studies of the effects of pre-existing damage that have been performed, have demonstrated an effect on the average number of new defects that form from impacts occurring on top of existing damage [28–31]. Gao *et al.* [29] studied the effects of cascade overlap in iron with primary knock-on (PKA) energies in the range 0.4 – 5 keV, and Stoller *et al.* [31] expanded the range by using 10 keV PKA energies. In both studies, a significant reduction in defect production was observed when cascades were simulated in already damaged systems. Furthermore, effects on the existing population of defects have also been demonstrated [32,33], including loop growth through dislocation climb, and loop annihilation, proving that nonlinearities in the primary damage production may be important in several respects. Cascades have also been shown to enhance the migration of existing defects [34,35], which in the long term leads to observable differences in damage build-up in different materials [36,37]. The interplay between defect formation and migration is thus critical for understanding damage evolution under irradiation. In this work, we focus on the aspect of the primary damage formation in the presence of radiation-induced defects.

In bcc materials, recent MD simulation work indicates that there is a significant difference in the damage produced in thin foils compared to bulk, with a major difference being the formation of vacancy clusters and loops close to the surface, large enough to be observable in experiments [38–40]. Large defects produced by ion irradiation of thin foils can be experimentally observed using transmission electron microscopes [38], which provides a good basis for direct comparison with atomistic simulations. However, in foils the proximity of a surface further complicates analysis of experimental results, since image forces may result in significant loop loss [41]. Osetsky *et al.* [39] also noted the lack of larger interstitial clusters in the primary damage as a result of migration, and described a mechanism for vacancy loops gliding along $1/2\langle 111\rangle$ directions to the surface.

Previous studies that have been conducted of overlapping cascades have focused on low energy cascades in iron and iron alloys. Although tungsten (W) is the current material of choice for many components in future fusion reactors, to our knowledge no studies of overlapping cascades in W exist in the literature.

Since the state of the material at the time of an impact depends on the dose rate, irradiation temperature, and the migration and trapping of defects under those circumstances, the question of what type of disorder exists at the time of impact is non-trivial. In this work, we study the damage production in cascades overlapping the primary damage of previous cascades, in both bulk and thin foils of α-Fe and W. We consider here the limit of zero thermal evolution between cascades. To address the question of how sensitively the configuration of the pre-existing damage affects results, we have simulated several different initial damage states, also studying the effects of SIA- and vacancy-type defects separately. In order to extend previous work, and probe the limits of the possible effects of overlap on defect structures under energetic neutron and ion irradiation, we investigate the damage from energetic cascades at or above the subcascade splitting threshold of each material. For this purpose, we have used 50 keV PKAs in iron, and 150 keV PKAs in tungsten. Above the subcascade splitting threshold, cascade effects become linear in cascade energy, hence no new physics is expected above that level.

2. Methods and analysis

Full collision cascades were simulated in cells containing defects from prior cascades. We performed 40 overlapping cascades on each configuration in Fe, and 20 on each configuration in W. The initial damage for all of the cases is presented in the Supplementary material. Details of the pre-existing defects contained in the cells are listed in Table 1. A number of initial damage configurations were chosen based on the following criteria: (i) damage dominated by point defects, with very little clustering (denoted in the following as "low damage"), (ii) damage characterized by a high degree of clustering relative to primary damage in the material in question (denoted in the following as "high damage"), (iii) only vacancies

Table 1
Details of the defects contained in the pre-existing damage.

Material	N_{SIA}	N_{vac}	$N^{SIA}_{maxclust}$	$N^{vac}_{maxclust}$
Fe bulk high damage (1)	162	162	29	64
Fe bulk high damage (2)	196	196	67	45
Fe bulk low damage	87	87	8	6
Fe bulk vac only	0	227	0	35
Fe bulk SIA only	210	2	47	1
Fe foil high damage	51	383	5	248
Fe foil low damage	105	112	5	5
W bulk high damage	228	228	76	50
W bulk low damage	129	129	73	5
W foil high damage	153	922	84	646
W foil low damage	206	218	65	6

(created by removing atoms in a perfect lattice from sites corresponding to empty Wigner-Seitz cells in the actual primary damage of chosen cascades, and relaxing), and (iv) only SIAs and interstitial clusters (for this, vacancies from the initial damage were removed by inserting atoms into the empty Wigner-Seitz cells and relaxing).

These damage configurations were chosen in order to investigate the effects of overlap in a range of irradiation conditions and varying local dislocation microstructure. Although the larger defect configurations were the product of athermal formation in a cascade, the high energy of a directly overlapping cascade means that the exact configuration of the clusters is less important than their size and point defect density. Hence we consider these configurations representative also of a slightly evolved microstructure, where larger defect clusters form thermally. In order to capture the effects of direct overlap of a cascade with pre-existing damage, the overlapping recoils were initiated in a direction aimed towards the initial damage.

We have investigated effects in both bulk cascade events and near-surface cascades in thin foils. For foil simulations, a free surface was modelled by setting open boundaries in one dimension, otherwise periodic boundaries were applied in all directions. A Berendsen thermostat [42] scaling the temperature towards 0 K was applied to a unit cell thick region along the periodic borders of the systems, to mimic the natural heat dissipation, and inhibit self-interaction of cascades over the periodic boundaries. We have previously shown that this approach gives damage production results not dependent on the cell size or choice of thermostat parameter [43]. In Fe, the bottom layers of the cell in surface simulations were fixed, and the border thermostat was applied to the region immediately above it, to emulate the bulk below the sample. In W, on the other hand, the full depth of TEM thin foils was simulated, with open surfaces on both top and bottom. We chose this set-up for W simulations, since ions penetrate through a significant portion of the foil, and the primary damage is directly comparable with experimental observations in this material [6,44]. Such comparison is beyond the scope of the current article, but will be the focus of future work. Both the bulk and thin foil Fe systems contained 3.456 million atoms ($120a \times 120a \times 120a$). The W bulk cells contained 6.75 million atoms, while foil simulation cells contained over 13 million atoms. The cascades in Fe and in bulk W were evolved for 40 ps, which was sufficient to allow the cascade region to cool down to a few Kelvin. In W foil simulations, the time was extended to 60 ps, since dense near-surface cascades in W take longer to cool. In bulk, recoiling atoms were given random directions. For Fe foil simulations, a (001) surface was used, and the incident angle of the projectile was chosen close to 22°, with a slight random variation, corresponding to the experimental setup in Ref. [45]. In W, a (014) surface was used, and an incidence angle varied within 3° of 15°, to correspond to the experimental setup in Ref. [6]. In each case, the ion was initiated 5 Å above the surface. The simulations were carried out with the classical MD code PARCAS [46,68–70]. For Fe, we used the embedded atom method (EAM) potential by Ackland et al. [47], and for W the potential by Derlet et al. [48]. Both potentials were stiffened by smoothly joining them to the universal ZBL repulsive potential [49,50].

The surviving point defects were analysed using the Wigner-Seitz cell (W-S) method, to determine the positions and numbers of vacancies and interstitials in the damaged systems [51]. For thin foils, all atoms on top of the surface were considered adatoms, and all atoms further away from the surface than the potential cutoff were labelled as sputtered atoms. Both were disregarded in the subsequent analysis. The clustering of point defects was studied by considering two vacancies (or interstitials) to be in the same cluster if the distance between them was within a cutoff range. For vacancies, we used a cutoff range of $(r_{2NN} + r_{3NN})/2$, and for interstitials $(r_{3NN} + r_{4NN})/2$, where r_{NN} is the nearest neighbour distance, r_{2NN} is the second nearest neighbour distance, etc. The size-frequency distribution of defect clusters was found by binning the data on a logarithmic scale. Dislocations were identified using the DXA dislocation extraction algorithm [52] as implemented in Ovito [53].

3. Results

3.1. Defect numbers

We see an overall decrease in the numbers of defects produced from cascades overlapping previous damage in Fe, as compared to the numbers predicted from cascades in defect-free crystal, in agreement with earlier work [28,29,31,32]. At most, we observe a decrease of 40%, depending on the morphology of the pre-existing damage. For certain damage morphologies, the difference in total numbers of defects is only 10%, which is within the statistical uncertainty of around 10–15% in these results. In contrast, in W the differences in total defect numbers were in all cases less than the statistical uncertainty.

We also observe that the pre-existing damage in Fe causes a larger spread in the distribution of the final defect numbers, as compared to the initial damage distribution. This shift is shown in

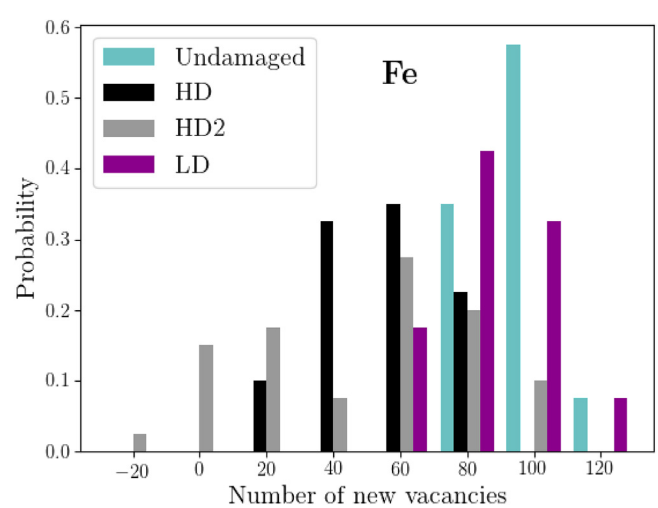

Fig. 1. Total numbers of new defects (numbers of vacancies equals numbers of SIA in bulk simulations) in 50 keV cascades in bulk Fe, for various initial conditions. The probability is obtained as the fraction of all simulated cascades that produce the indicated numbers of additional defects, counted in bins of width 20. Negative numbers occur when the net number of vacancies is lower than in the pre-existing damage.

the histogram in Fig. 1. This, again, is not observed in W. Furthermore, there is a clear effect of the morphology of the existing damage in Fe. In cells with larger defect clusters, we see the strongest decrease in the numbers of new defects.

In these bcc materials, interstitial clusters appear as clusters of crowdions, which are identifiable (by the DXA [54] algorithm) as dislocation loops when clusters contain more than 10–12 crowdions. We use this to compute the change in total dislocation line length D_l in the cell, shown in Fig. 2. There is a clear effect of the pre-existing damage in Fe, resulting in a larger spread of the distribution of dislocation line length from overlapping cascades, compared to single cascades. Cells with “low damage” had no pre-existing dislocations, hence only an increase is possible, as with the single cascade damage. However, both the pre-existing damage consisting of point defects, and that containing dislocation loops, caused more *new* dislocation line formation in overlapping cascades than that seen from single cascades. Hence, while the additional damage in later cascades is lower in terms of point defects, more large SIA clusters are formed than from two separate cascades. On the other hand, also a net decrease in the dislocation line length was possible. We do not see a similar effect of overlap in W, where the distribution of dislocation line length created in single and overlapping cascades is largely similar.

We find an effect of loop size in the process of growth or destruction of dislocation loops. Three outcomes of an overlapping cascade on existing defect clusters are possible: a) complete destruction of a defect; b) no effect on the defect, except slight cascade-induced migration in the case of SIAs; c) change in size and/or shape of defect cluster, including a possible change in the Burgers vector of loops. By analyzing where the cascade heat spikes have developed, we see that loops that are fully enveloped by the overlapping cascade have a very high probability of being destroyed, while a partial hit to the edge of a loop has a significant probability of increasing the loop size rather than decreasing it. Fig. 3 shows the change in dislocation length of individual loops in Fe, in cases where it was possible to identify a particular loop before and after the overlapping cascade. In the case of partial overlap by the liquid heat spike region, there is a significant chance that the loop will grow. As a loop grows, the chances of it being fully enveloped and hence destroyed by a later cascade diminishes quickly, while the probability of only partial overlap and survival grows.

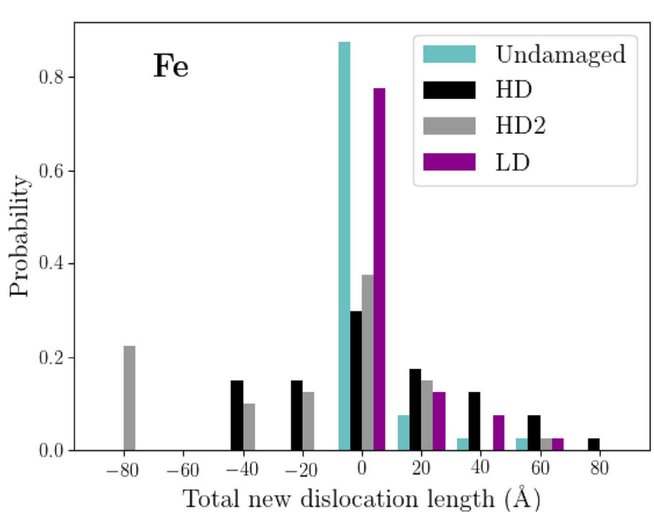

Fig. 2. Total new dislocation length from 50 keV cascades in bulk Fe, for various initial conditions. The probability is obtained as the fraction of all simulated cascades that produce the indicated additional dislocation length, counted in bins of width 20 Å. Negative numbers occur when the net dislocation length is lower than in the pre-existing damage.

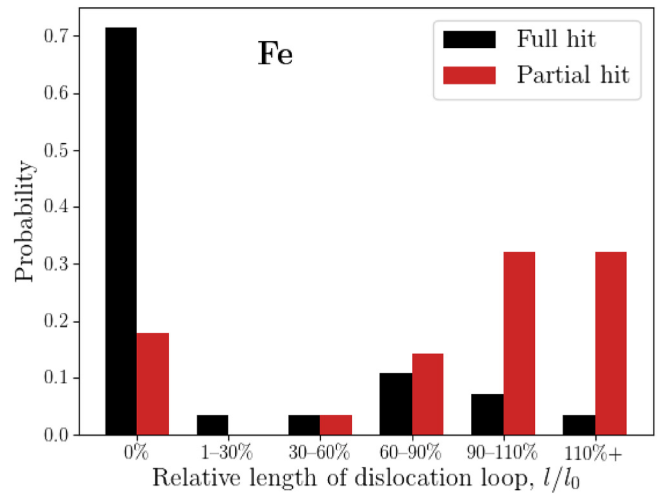

Fig. 3. Change in dislocation length of loops that are hit by the energetic, or “liquid” cascade region in Fe.

Vacancy clusters in the overlapping damage in Fe were also generally larger than those observed from single cascades. In the case of only vacancies in the pre-existing damage in Fe, the average size of the largest vacancy cluster was almost twice the size of the pre-existing 35 vacancy cluster. This indicates an effect of clustering of pre-existing vacancies, in agreement with [30]. At most, a cascade overlapping the pre-existing vacancy damage resulted in a cluster of 175 vacancies, which included a large fraction of the initial vacancies. This enhanced clustering effect is not observed when there are also interstitials present in the pre-existing damage, indicating that these interstitials recombine with the vacancies in the cascade core, reducing the number of vacancies available in the final defect cluster. The results for all cases are given in Table 2.

3.2. Cascade collapse

A striking effect of overlap in Fe is seen in the morphology of the vacancy defect population. MD investigations to date all report vacancy clusters as 3-dimensional configurations, with vacancy-type dislocation loops occurring only rarely in bcc materials. Only one instance of a vacancy-type dislocation loop in cascade simulations in Fe has been reported [55], which occurred once in 100 cascades. In the simulations reported here, no vacancy-type loops formed in the individual cascades. However, cascades which overlapped a dense pre-existing vacancy cluster formed a vacancy-type loop in 2 out of 40 cascades, and a partial loop once. An illustration

Table 2
Final defect numbers from overlapping cascades in bulk and foil, Fe and W. For cascades overlapping pre-existing defects, the number of *new* defects is given.

Material	Fe		W	
	N_{SIA}	N_{vac}	N_{SIA}	N_{vac}
bulk (perfect)	93.7±10.7	93.7±10.7	179±21.0	179±21.0
bulk high damage	54.6±18.0	54.6±18.0	168.4±16.5	168.4±16.5
bulk low damage	86.3±15.1	86.3±15.1	185.5±22.8	185.5±22.8
bulk SIA damage	80.4±16.2	80.4±16.2	193.6±21.1	193.6±21.1
bulk vac damage	79.8±15.1	79.8±15.1	170.4±23.9	170.4±23.9
foil (perfect)	84.5±14.8	142.7±81.2	120.9±8.9	545.4±94.9
foil high damage	70.0±20.2	124.7±87.1	62.4±18.2	265.3±104.0
foil low damage	70.2±16.4	140.8±147.8	64.2±21.1	667.0±178.9

of this is presented in Fig. 4, showing the defects before and after an overlapping cascade in Fe.

Hence vacancy loop formation appears significantly more likely as a result of cascade overlap than from individual cascades in Fe. The Burgers vector of the vacancy-type loop formed after a secondary cascade was once ⟨100⟩ and once 1/2⟨111⟩. In W, we did not observe cascade collapse as a result of cascade overlap, despite the presence of a dense vacancy cluster in the pre-existing damage. This may be due to the relatively few times that the subsequent cascades directly overlapped the vacancy cluster, since cascades develop in random, uncontrollable directions and were nevertheless spatially fairly concentrated.

3.3. Surface effects

Similarly to single cascades in foils [40], the effect of a nearby surface in these overlapping cascades was strongest on the vacancy population. We observe a large variation in the numbers and morphology of the overlapping damage, which mirrors a similar variation in the primary damage morphology of single cascades.

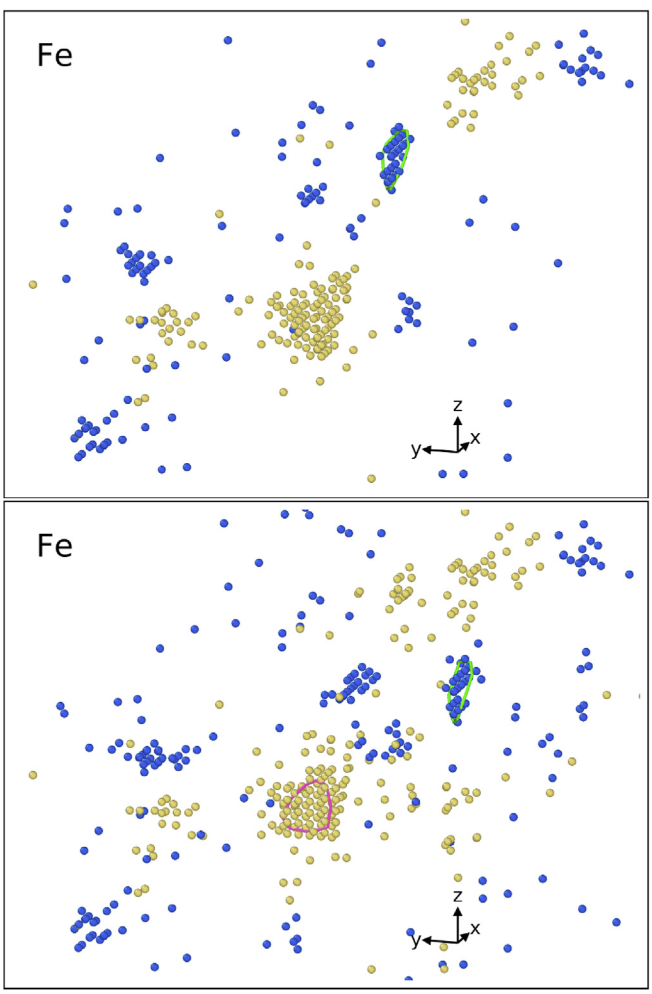

Fig. 4. Illustration of overlap-induced cascade collapse in Fe. Yellow spheres indicate empty Wigner-Seitz cells (vacancies) and blue spheres indicate multiply occupied Wigner-Seitz cells (SIAs). Green lines mark dislocation loops with 1/2⟨111⟩ Burgers vector, and magenta lines mark loops with ⟨100⟩ Burgers vector. (top) Pre-existing damage including a dense 3-dimensional vacancy cluster. (bottom) Primary damage after overlapping cascade. The vacancy cluster has condensed into a vacancy type ⟨100⟩ loop. (For interpretation of the references to color in this figure legend, the reader is referred to the Web version of this article.)

The variation in vacancy numbers stems from occasional cascades that develop right at the sample surface. These give rise to a long tail in the distribution of damage from individual ions, resulting in up to 800 vacancies at best in these simulations. The distribution of (new) defect numbers shifts slightly towards fewer interstitial defects in overlapping cascades, while for vacancies the distribution widens, showing an even larger spread in results compared to cascades in undamaged foil. The distributions are shown in Fig. 5.

The strongest effect of surface damage was seen on the number of new vacancies in W foils with a large vacancy cluster in the pre-existing damage. This large underdense area inhibited further massive ejection of material, which is the main cause of large near-surface vacancy clusters. Hence the average count of new vacancies in the overlapping damage is much lower than in pristine foil.

3.4. Size-frequency distributions

In Fe, where point defects dominate the damage in single cascades, we observe a slight decrease in the number of new single defects, and a corresponding increase in the frequency of larger clusters.

Since the initial defects in the pre-damaged cell does not represent the statistical distribution of single cascades on average, and furthermore was purposely chosen to be dominated by one or the other end of the size spectrum, we have separated this from the

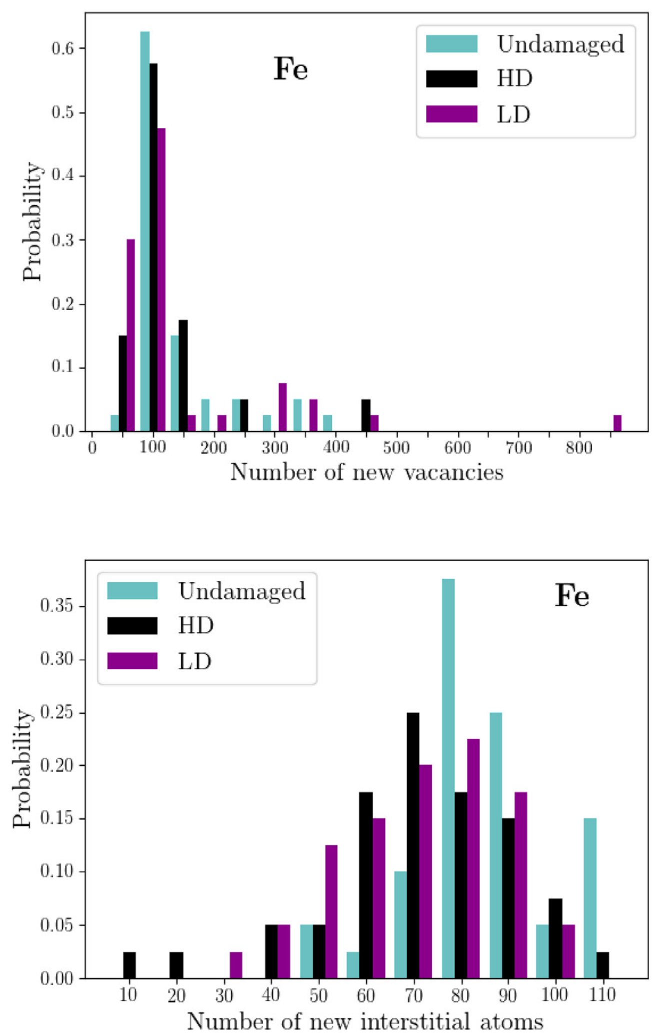

Fig. 5. Total numbers of new defects in foil simulations in Fe.

analysis of the statistics of the damage produced from the overlapping cascade. In interpreting these results, however, it is important to note that separating prior damage from new damage is not straightforward, due to the frequent transformation of existing damage. Hence, in analysing the distribution of defect sizes of the additional damage, we subtracted from the final defect count the numbers of defects that had existed in the initial damage. For example, where the initial damage contained a loop of size $N = 40$, one defect was subtracted from the total count in the bin with defects of size $N = 30-70$. In this way, the results portray the damage that would ideally be inserted as additional damage from a cascade event in a larger scale simulation, such as in OKMC microstructural evolution, when the fluence is such that cascades overlap with existing defects. The distributions are shown in the plots in Figs. 6 and 7.

3.5. Structure of defects

Complex defect structures are formed as the heat spike overlaps with existing damage. This is particularly the case in W, where defects are in general larger than in Fe, and complex configurations are observed already in the damage from two overlapping impacts.

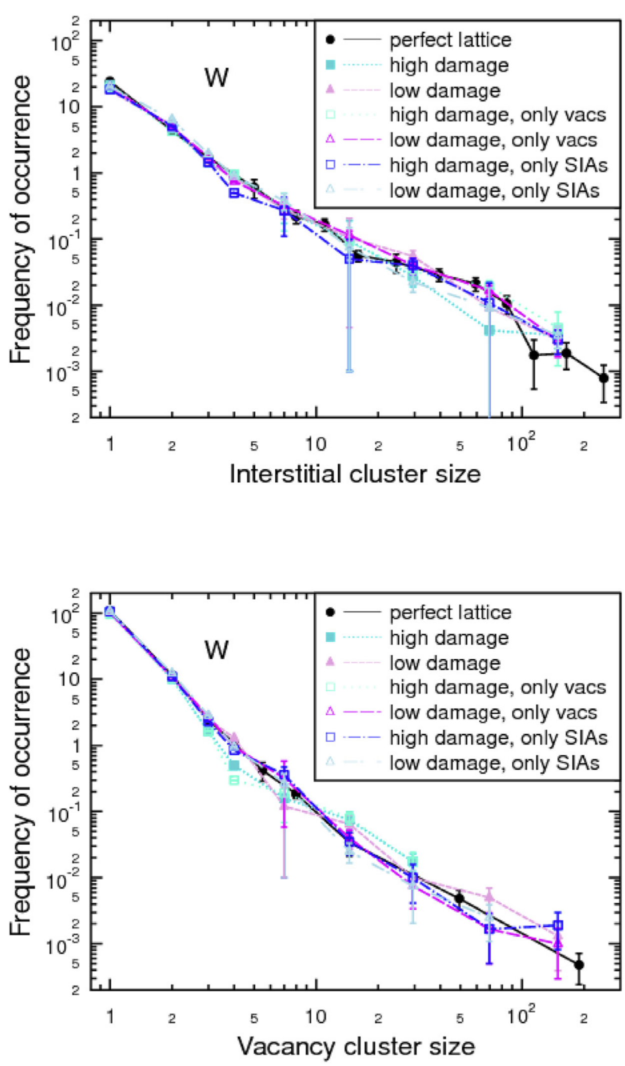

Fig. 6. Size-frequency distributions for additional defect clusters produced in overlapping cascades in bulk W.

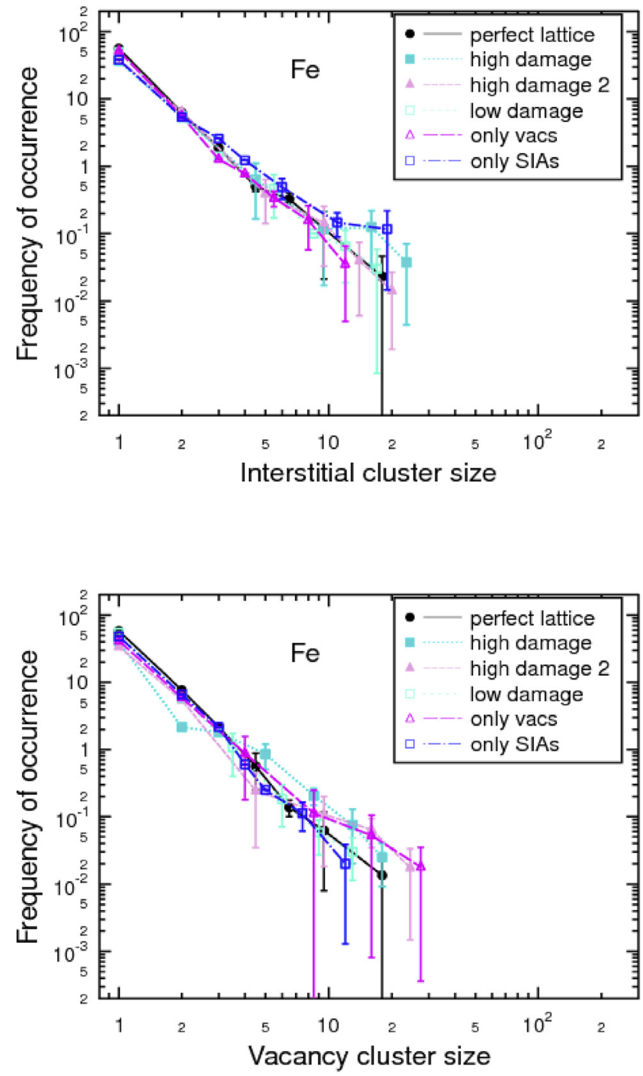

Fig. 7. Size-frequency distributions for additional defect clusters produced in overlapping cascades in bulk Fe.

The mechanism for formation of these novel defects can be seen from inspection of the energetic atoms contained in the heat spike during the development of the second cascade. It is observed that the more complex defects form when this “melted” region partially encompases a defect, leaving part of it untouched on the outside of the cascade, and reconnecting the dislocation line in an arbitrary manner as the cascade volume recrystallizes. This process is depicted for one such occurrence in Fig. 8. A similar increase in complexity of the morphology of pre-existing defects occurred almost every time that a dislocation loop experienced partial overlap with a cascade.

Figs. 9–12 show some of the novel defects found in the debris of the overlapping cascades. Lines indicate dislocations (analyzed using Ovito's DXA [53]), while spheres mark defects found using a Wigner-Seitz analysis. The top picture in each figure shows the Burgers vector of the lines, green lines have $\mathbf{b} = 1/2\langle 111\rangle$ while pink lines have $\mathbf{b} = \langle 100\rangle$. The grey surfaces show areas of disordered lattice as identified in the DXA dislocation analysis; this includes the sample surface. (Note that the DXA algorithm identifies the extended strain field of individual crowdions as a large defect volume - it is clear from an energy filtered analysis of the atoms (not pictured here) that these are simply the crowdion string with

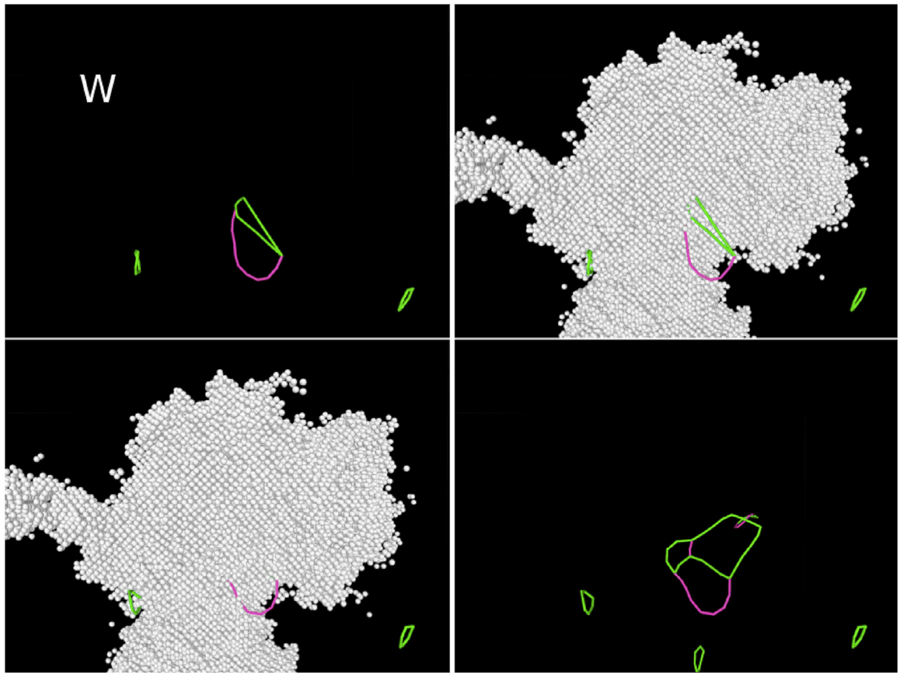

Fig. 8. Morphology change of a pre-existing defect in W that is partially hit by the energetic, or "liquid" cascade region. (top left) Dislocation lines marking pre-existing defects. Green lines indicate dislocations with $1/2\langle 111\rangle$ Burgers vector and magenta indicates a $\langle 100\rangle$ Burgers vector. (top right) Atoms of liquid phase at the point of maximum extent of the heat spike of an overlapping cascade superimposed on the pre-existing damage. (bottom left) Atoms of liquid phase superimposed on dislocation lines of final damage from overlapping cascade. (bottom right) Dislocation lines in final damage. All dislocations visualized using the DXA algorithm [54] in Ovito [53]. (For interpretation of the references to color in this figure legend, the reader is referred to the Web version of this article.)

no additional disorder.) Blue spheres mark SIAs as identified by a Wigner-Seitz analysis, while yellow spheres represent vacant sites and red spheres mark adatoms that have been pushed above the surface as a result of the heat spike. In the bottom pictures, lines are colored according to their edge/screw nature, with red indicating screw and blue edge; the white is an even mixture of screw and edge. Arrows attached to the lines show the direction of the Burgers vector, and for clarity the grey surfaces have been removed.

Fig. 9 shows a dislocation network joining two clusters of interstitials by screw dislocation segments. A similar occurrence of screw dislocations has not been observed from single cascades. Although the existence of the screw segments is energetically unfavourable, and not forced by the presence of excess material such as is the case for the edge-type dislocation loops, relaxation of this configuration would require the transformation of the Burgers vector of either of the end edge dislocations. Hence the energy barrier for this process is non-negligible, and relaxation into a pure edge dislocation would require either time or high temperature, rendering this configuration momentarily stable, and sessile. We note that such a configurationally bound extended defect structure will not be found with a standard Wigner-Seitz analysis alone, nor will the size of the defect be accurately captured by considering only the numbers of point defects, nor indeed by a cluster analysis with the typical cut-off around 2NN distance. In this case a dislocation analysis such as the DXA algorithm [54] implemented in Ovito [53] is essential. Defects with this type of structure were nevertheless sufficiently rare in these simulations, that we have disregarded the few occurrences in the size-frequency cluster analysis presented above.

Another type of defect configuration not previously observed in single cascades is shown in Fig. 10. This network of dislocation segments is essentially 3-dimensional, with roughly the form of a tetrahedron. As such, this defect is sessile, and very stable due to the two $\langle 100\rangle$ edge segments. A test of its stability proved that it does not transform even at 1000 K over the duration of 2 nano seconds.

Overlapping cascades near the surface of thin foils also showed novel dislocation structures, with dislocation lines beginning at the surface, or in a near-surface void, and often extending several nanometers into the material. Such dislocation lines often have a strong screw element, and can be both of interstitial or vacancy type. Fig. 11 shows a large dislocation of interstitial type extending from the surface down to a depth of about 7 nm, where it is on one side efficiently pinned by a $\langle 100\rangle$ edge dislocation segment.

Vacancy type dislocation loops are observed with higher frequency than in individual cascades, but still mainly near the surface in the foil irradiation simulations. One network of vacancy type dislocations is pictured in Fig. 12. All vacancy-type dislocation loops observed in W were connected to voids or disordered vacancy-rich areas, effectively immobilizing the loop. No clear cascade collapse was observed.

4. Discussion

The observed formation of vacancy-type dislocation loops in the overlap debris in Fe proves that the general lack of vacancy-type loops in cascade simulations in bcc materials is not due to an intrinsic property of the interatomic potentials, but that vacancy-type loops can and do form in MD simulations given the right conditions. The same interatomic potential did not produce vacancy-type dislocation loops from any of the 40 individual cascades in bulk Fe simulated in this work. Hence our results support the notion of cascade collapse from cascade overlap in Fe, postulated based on experimental evidence in the 80's [3,4].

The effect of overlap on the size distribution of the dislocation loop population, which is observed in Fe, is not seen in the simulations in W, where the distribution of total (new) dislocation line length is largely similar for single and overlapping cascades. We

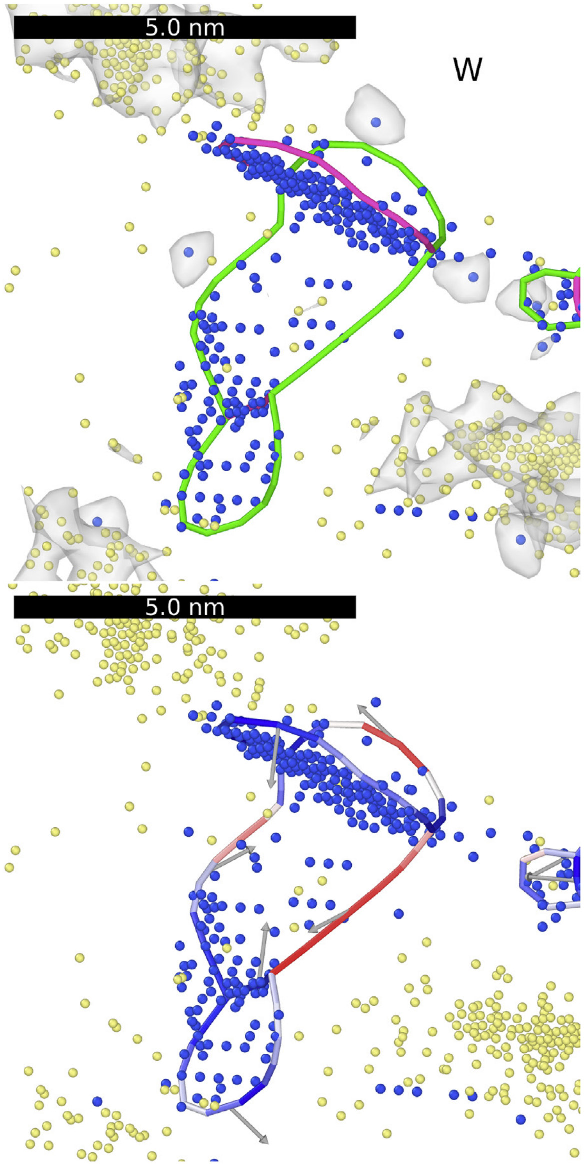

Fig. 9. (Color online) A complex extended defect formed in bulk W from two overlapping cascades. (top) Green lines indicate dislcoation segments with a $1/2\langle 111\rangle$ Burgers vector and magenta lines indicate a $\langle 100\rangle$ Burgers vector. (bottom) Red lines indicate a shear dislocation and blue lines indicate an edge dislocation. White lines mark a mixed (shear/edge) region of the dislocation line. Blue spheres mark multiply occupied Wigner-Seitz cells (indicating SIAs) while yellow spheres mark empty Wigner-Seitz cells (indicating vacancies). The gray surface (top) encloses regions of strongly distorted lattice. All dislocations and isosurface visualized using the DXA algorithm [54] in Ovito [53]. (For interpretation of the references to color in this figure legend, the reader is referred to the Web version of this article.)

attribute this to the different nature of high-energy cascades in Fe and W. In Fe, cascades start splitting into subcascades at around 20–30 keV [8], while in W subcascade splitting begins at around 150 keV [7]. Due to the subcascade splitting, energetic cascades in Fe are most often spatially spread out, with relatively low energy density compared to cascades in W. To quantify the effective energy density in the cascades studied here, we use the method of component analysis described in Ref. [56]. Briefly, an ellipsoid is found, that contains the cascade, and the volume of the ellipsoid is taken as the effective volume of the cascade. This method has typically been used only to analyze the spatial distribution of the final defects in cascades (see also [57]), but here we are interested

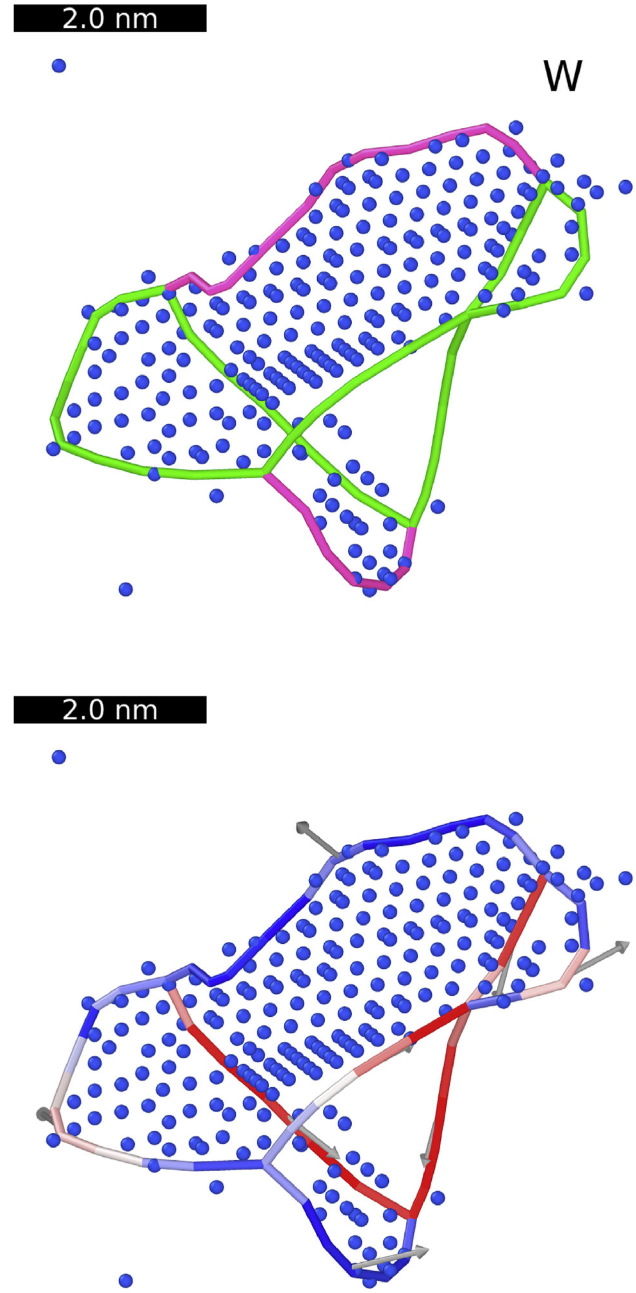

Fig. 10. (Color online) A 3-dimensional dislocation network formed in bulk W from two overlapping cascades. (top) Green lines indicate dislcoation segments with a $1/2\langle 111\rangle$ Burgers vector and magenta lines indicate a $\langle 100\rangle$ Burgers vector. (bottom) Red lines indicate a shear dislocation and blue lines indicate an edge dislocation. White lines mark a mixed (shear/edge) region of the dislocation line. Blue spheres mark multiply occupied Wigner-Seitz cells (indicating SIAs) while yellow spheres mark empty Wigner-Seitz cells (indicating vacancies). The gray surface (top) encloses regions of strongly distorted lattice. All dislocations and isosurface visualized using the DXA algorithm [54] in Ovito [53]. (For interpretation of the references to color in this figure legend, the reader is referred to the Web version of this article.)

in the density fluctuations arising in the liquid core of the cascade, and not in the final defects per se (for example, interstitials resulting from replacement collision sequences are not of interest to us in this analysis, and on the other hand, we do not want to exclude regions where the damage may have recombined). Thus we instead calculate the effective volume of the liquid-like core region. To do this, we perform the component analysis on the atoms with

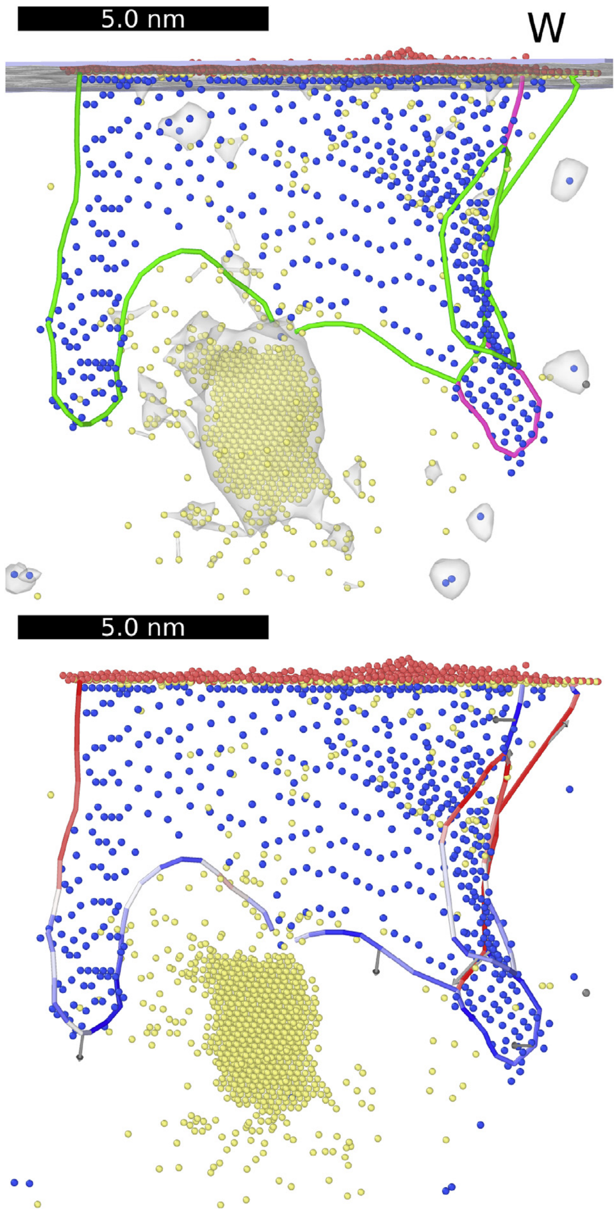

Fig. 11. (Color online) An extended interstitial-type dislocation in W foil formed from two overlapping cascades. (top) Green lines indicate dislcoation segments with a 1/2⟨111⟩ Burgers vector and magenta lines indicate a ⟨100⟩ Burgers vector. (bottom) Red lines indicate a shear dislocation and blue lines indicate an edge dislocation. White lines mark a mixed (shear/edge) region of the dislocation line. Blue spheres mark multiply occupied Wigner-Seitz cells (indicating SIAs) while yellow spheres mark empty Wigner-Seitz cells (indicating vacancies). The gray surface (top) encloses regions of strongly distorted lattice. All dislocations and isosurface visualized using the DXA algorithm [54] in Ovito [53]. (For interpretation of the references to color in this figure legend, the reader is referred to the Web version of this article.)

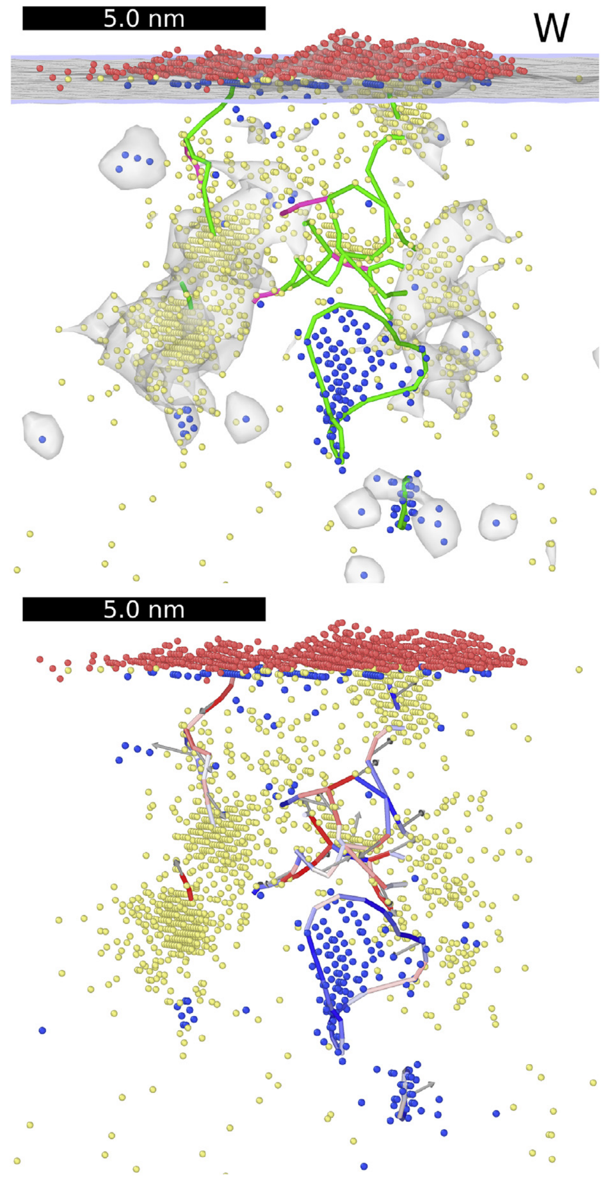

Fig. 12. (Color online) A complex network of vacancy-type dislocations in W foil, formed from two overlapping cascades. Dislocation lines terminate in disordered, vacancy rich areas. (top) Green lines indicate dislcoation segments with a 1/2⟨111⟩ Burgers vector and magenta lines indicate a ⟨100⟩ Burgers vector. (bottom) Red lines indicate a shear dislocation and blue lines indicate an edge dislocation. White lines mark a mixed (shear/edge) region of the dislocation line. Blue spheres mark multiply occupied Wigner-Seitz cells (indicating SIAs) while yellow spheres mark empty Wigner-Seitz cells (indicating vacancies). The gray surface (top) encloses regions of strongly distorted lattice. All dislocations and isosurface visualized using the DXA algorithm [54] in Ovito [53]. (For interpretation of the references to color in this figure legend, the reader is referred to the Web version of this article.)

kinetic energies above 0.5 eV existing at the time of maximal extent of the liquid region. This occurs at the end of the ballistic phase, at around 300 fs for 150 keV cascades in W [58], and slightly earlier for 50 keV cascades in Fe. At this time, the full spatial extent of the cascade is determined, after which the various regions start equilibrating and cooling. Determined in this way, the energy density (eV/atom) in 150 keV cascades in W is a factor of 2.4 larger than that in 50 keV cascades in Fe. (The values are 6.12e-3 and 2.55e-3 for W and Fe, respectively.) Increasing the PKA energy in Fe would only serve to decrease this quantity, due to the effect of subcascade splitting. The spatial extent of the ballistic phase is illustrated in Fig. 13 for two typical 200 keV cascades. The fluctuations in material density resulting from a single cascade in Fe are thus fairly small, stemming from small disordered pockets each caused by only 20–30 keV deposited kinetic energy. As a result, even energetic cascades in Fe mainly form point defects, with occasional small clusters. The overlapping cascades are then subsequently also sensitive to the dense and underdense regions that exist prior to the cascade, due to the presence of point defects. In W, on the other hand, the heat spikes in 150 keV cascades are compact, and the high energy density allows significant fluctuations to

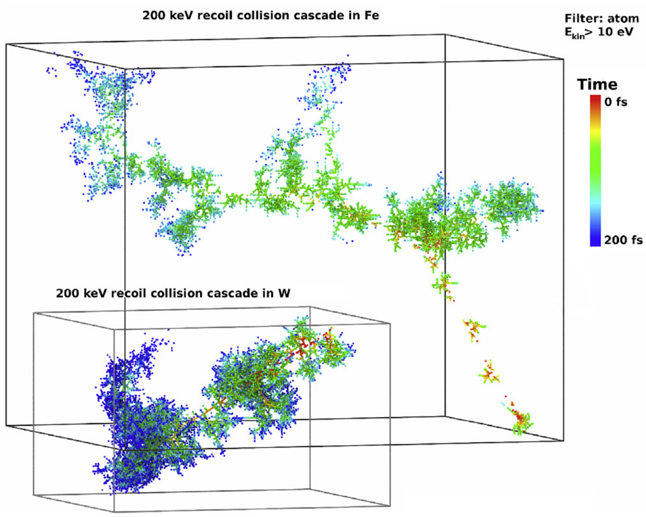

Fig. 13. (Color online) The spatial extent of ballistic atoms in typical 200 keV cascades, in W and in Fe. Atoms from different times are superimposed in the same image, with coloring according to the time when they exist in that location. Only atoms with kinetic energies above 10 eV are shown. Both cascades are rendered in the same scale. (For interpretation of the references to color in this figure legend, the reader is referred to the Web version of this article.)

appear in the material density within the heat spike, resulting in large dislocation loops forming with a high probability. The relative population of single defects is correspondingly smaller than in Fe. A subsequent overlapping cascade thus creates new defects largely independently of the initial state of the material.

The occurrence of novel defects, including ⟨100⟩- type dislocation loops of both vacancy and interstitial [59] nature, in the primary damage of overlapping cascades in Fe can also be explained by the existence of regions with excess material prior to the second cascade. When a cascade overlaps with a pre-existing defect cluster, the excess material (or under-dense region) required for the in-cascade formation of dislocation loops will be already present, and will with high likelyhood condense into a dislocation loop of comparable size to the original point defect cluster, or larger. The observation that dislocation loops only start to appear in Fe in significant numbers after cascade overlap is also well in line with the experimental observations comparing damage production in Ni, Cu and Fe [4,60–62]. These experiments showed that visible damage appears in BCC Fe at much higher doses than in the FCC metals Cu and Ni. In Cu and Ni, there is compelling evidence that single cascades can produce TEM-visible extended defects [10,63]. On the other hand, recent experiments and simulations (on which the W part of this work is based) showed that also in W, large TEM-visible loops can be produced in single cascades [6,7]. Combination of these observations with the results of the current work shows that the crucial difference between Fe and Cu or Ni stems not from the crystal structure, but from the cascade density. The cascade density can be increased by introducing heavier PKAs, and this has been shown to produce TEM-visible defects in Fe at much lower fluence than from self-ion irradiation [9], a finding which is supported by simulations [64].

Furthermore, although different interatomic potentials predict different stabilities for defect clusters of various morphologies [16], it is important to note that the morphology of clusters formed in cascades is in general not determined by the lowest energy configuration predicted by a given potential. In particular, in W, dislocation loops of both ⟨100⟩ and 1/2⟨111⟩ Burgers vector form routinely with the same potential [65]. Hence small differences in predictions of the stability of different loops, and C15 clusters in Fe [66,67], is in and of itself not likely to change this picture.

In W, fairly large defects are frequently formed already in single cascades. For these defects that span several nanometers, partial overlap with a successive cascade becomes more likely than in the case of very small defects. As the overlapping cascade then recrystallizes, the dislocation lines entering the liquid region must necessarily be continued, and due to the disorder in the cascade core, configurations that are "frozen in" may be arbitrarily complex. Due to the high frequency of defects of significant size from single cascades in W, the formation of such complex, sessile defects is frequent already at the first stages of cascade overlap, as a result of just two successive impacts.

5. Conclusions

In conclusion, we have found an effect of pre-existing defects on the statistics of the primary radiation damage in Fe. On average, fewer defects were created in overlapping cascades, although we do note a dependence of this effect on the morphology of the pre-existing damage. Dense clusters of pre-existing defects had a stronger impact than more evenly distributed point defects, on both the numbers of new defects and the distribution of sizes of the resulting defects in Fe. In the presence of larger defect clusters, occasionally cascades only caused the recombination of defects, and hence resulted in a net reduction of defect numbers. On average, however, the numbers increased in this study, where we have focused on the initial stage of overlap, where defects from only one or two previous cascades were present in the sample.

A striking effect of overlap in Fe was found in the frequent formation of vacancy-type dislocation loops when cascades overlapped with a pre-existing dense vacancy cluster, indicating that cascade collapse can be induced by cascade overlap.

In contrast to Fe, the average numbers and distributions of defects in W were not affected, to within the statistical uncertainties of this study. Instead, we observe a significant impact on the morphology of the defects, with complex structures appearing, including dislocation networks and screw dislocation lines connecting defects. This effect on the defect morphology alters the mobility of the defects, and may hence have a significant impact on the microstructural evolution.

The differences in overlap effect in Fe and W is attributed to the different nature of the cascades, with cascades in Fe splitting at relatively low PKA energy, and hence producing mainly point defects and small clusters. In contrast, the compact cascades in W produce frequent large defects in each individual event. Hence the potential to form large clusters is inherent in each cascade, and the process is less sensitive to whether there exists damage from before.

The damage from overlapping cascades varies strongly, and in addition is dependent on the morphology of the pre-existing damage. Thus there is a need for a more systematic study of the impact of different types of defect clusters, to provide detailed quantitative information of overlap effects at higher dose, for e.g. OKMC simulations of microstructural evolution under irradiation, as well as for rate theory calculations.

Data availability

The raw and processed data required to reproduce these findings cannot be shared at this time as the data also forms part of an ongoing study.

Acknowledgements

This work has been carried out within the framework of the EUROfusion Consortium and has received funding from the Euratom research and training programme 2014–2018 under grant agreement No 633053. The views and opinions expressed herein do not necessarily reflect those of the European Commission. AES acknowledges support from the Academy of Finland through project No. 311472. Grants of computer time from the CSC - IT center in Espoo, Finland, are gratefully acknowledged.

Appendix A. Supplementary data

Supplementary data related to this article can be found at https://doi.org/10.1016/j.jnucmat.2018.08.049.

References

[1] G. Was, Fundamentals of Radiation Materials Science: Metals and Alloys, Springer London, Limited, 2007.
[2] S. Zinkle, G. Was, Acta Math. 61 (2013) 735–758. The Diamond Jubilee Issue.
[3] A. Dunlop, B. Pande, K. Böning, P. Rosner, H. Schaefer, J. Nucl. Mater. 108–109 (1982) 83–94.
[4] I.M. Robertson, W.E. King, M.A. Kirk, Scripta Metall. 18 (1984) 317–320.
[5] R. Schäublin, B. Décamps, A. Prokhodtseva, J. Löffler, Acta Mater. 133 (2017) 427–439.
[6] X. Yi, A.E. Sand, D.R. Mason, M.A. Kirk, S.G. Roberts, K. Nordlund, S.L. Dudarev, Europhys. Lett. 110 (2015) 36001.
[7] A.E. Sand, D.R. Mason, A.D. Backer, X. Yi, S.L. Dudarev, K. Nordlund, Materials Research Letters 5 (2017) 357–363.
[8] R.E. Stoller, L.R. Greenwood, J. Nucl. Mater. 271–272 (1999) 57–62.
[9] M.L. Jenkins, C.A. English, B.L. Eyre, Philos. Mag. A 38 (1978) 97–114.
[10] M. Kirk, I. Robertson, M. Jenkins, C. English, T. Black, J. Vetrano, J. Nucl. Mater. 149 (1987) 21–28.
[11] T.M. Robinson, M.L. Jenkins, Philos. Mag. A 43 (1981) 999–1015.
[12] B.C. Masters, Philos. Mag. A: A Journal of Theoretical Experimental and Applied Physics 11 (1965) 881–893.
[13] C.A. English, B.L. Eyre, M.L. Jenkins, Nature 263 (1976) 400–401.
[14] I. Rovelli, S. Dudarev, A. Sutton, arXiv:1802.04556v1 [cond-mat.mtrl-sci] (2018).
[15] X. Yi, M.L. Jenkins, M.B. no, S.G. Roberts, Z. Zhou, M.A. Kirk, Phil. Mag. 93 (2013) 1715–1738.
[16] M.R. Gilbert, S.L. Dudarev, P.M. Derlet, D.G. Pettifor, J. Phys. Condens. Matter 20 (2008) 345214.
[17] P.M. Derlet, M.R. Gilbert, S.L. Dudarev, Phys. Rev. B 84 (2011) 134109.
[18] K. Arakawa, T. Amino, H. Mori, Acta Mater. 59 (2011) 141–145.
[19] N. Soneda, T.D. de la Rubia, Philos. Mag. A 78 (1998) 995–1019.
[20] C. Domain, C. Becquart, L. Malerba, J. Nucl. Mater. 335 (2004) 121–145.
[21] C.J. Ortiz, M.J. Caturla, Phys. Rev. B 75 (2007) 184101.
[22] D.R. Mason, X. Yi, M.A. Kirk, S.L. Dudarev, J. Phys. Condens. Matter 26 (2014) 375701.
[23] G. Nandipati, W. Setyawan, H.L. Heinisch, K.J. Roche, R.J. Kurtz, B.D. Wirth, J. Nucl. Mater. 462 (2015) 338–344.
[24] N. Castin, A. Bakaev, G. Bonny, A. Sand, L. Malerba, D. Terentyev, J. Nucl. Mater. 493 (2017) 280–293.
[25] R.S. Averback, T. Diaz de la Rubia, in: H. Ehrenfest, F. Spaepen (Eds.), Solid State Physics, 51, Academic Press, New York, 1998, pp. 281–402.
[26] L. Malerba, J. Nucl. Mater. 351 (2006) 28–38.
[27] R.E. Stoller, Comprehensive Nuclear Materials, Elsevier, Oxford, 2012, pp. 293–332.
[28] A.J.E. Foreman, W.J. Phythian, C.A. English, Philos. Mag. A 66 (1992) 671–695.
[29] F. Gao, D.J. Bacon, A.F. Calder, P.E.J. Flewitt, T.A. Lewis, J. Nucl. Mater. 230 (1996) 47–56.
[30] K. Nordlund, R.S. Averback, Phys. Rev. B 56 (1997) 2421–2431.
[31] R.E. Stoller, S.G. Guiriec, J. Nucl. Mater. 329–333 (Part B) (2004) 1238–1242.
[32] D. Terentyev, K. Vörtler, C. Björkas, K. Nordlund, Nucl. Instrum. Meth. B 259 (2007) 853.
[33] A.V. Korchuganov, V.M. Chernov, K.P. Zolnikov, D.S. Kryzhevich, S.G. Psakhie, Inorg. Mater.: Applied Research 7 (2016) 648–657.
[34] N.A. Capps, Molecular Dynamics Simulations of cascade Evolution Near Pre-existing Defects, Master's thesis, University of Tennessee, 2013.
[35] A.V. Korchuganov, K.P. Zolnikov, D.S. Kryzhevich, V.M. Chernov, S.G. Psakhie, AIP Conference Proceedings 1683 (2015), 020095.
[36] F. Granberg, K. Nordlund, M.W. Ullah, K. Jin, C. Lu, H. Bei, L.M. Wang, F. Djurabekova, W.J. Weber, Y. Zhang, Phys. Rev. Lett. 116 (2016) 135504.
[37] S. Zhang, K. Nordlund, F. Djurabekova, F. Granberg, Y. Zhang, T. Wang, Mater. Res. Lett. 5 (2017) 433–439.
[38] M.J. Aliaga, R. Schäublin, J.F. Löffler, M.J. Caturla, Acta Mater. 101 (2015) 22–30.
[39] Y.N. Osetsky, A.F. Calder, R.E. Stoller, Curr. Opin. Solid State Mater. Sci. 19 (2015) 277–286.
[40] A.E. Sand, M.J. Aliaga, M.J. Caturla, K. Nordlund, Europhys. Lett. 115 (2016) 36001.
[41] A. Prokhodtseva, B. Décamps, R. Schäublin, J. Nucl. Mater. 442 (2013) S786–S789.
[42] H.J.C. Berendsen, J.P.M. Postma, W. F. v. Gunsteren, A. DiNola, J.R. Haak, J. Chem. Phys. 81 (1984) 3684–3690.
[43] J. Samela, J. Kotakoski, K. Nordlund, J. Keinonen, Nucl. Instrum. Meth. Phys. Res. B 239 (2005) 331–346.
[44] D. Mason, A. Sand, X. Yi, S. Dudarev, Acta Mater. 144 (2018) 905–917.
[45] A. Prokhodtseva, B. Décamps, R. Schäublin, J. Nucl. Mater. 442 (2013) S786–S789.
[46] K. Nordlund, Parcas Computer Code. The Main Principles of the Molecular Dynamics Algorithms Are Presented in [69,68]. The Adaptive Time Step Is the Same as in [70], 2010.
[47] G.J. Ackland, M.I. Mendelev, D.J. Srolovitz, S. Han, A.V. Barashev, J. Phys. Condens. Matter 16 (2004) S2629–S2642.
[48] P.M. Derlet, D. Nguyen-Manh, S.L. Dudarev, Phys. Rev. B 76 (2007), 054107.
[49] J.F. Ziegler, U. Littmark, J.P. Biersack, The Stopping and Range of Ions in Solids, Pergamon, New York, 1985.
[50] C. Björkas, K. Nordlund, S.L. Dudarev, Nucl. Instrum. Meth. B 267 (2009) 3204–3208.
[51] K. Nordlund, M. Ghaly, R.S. Averback, M. Caturla, T. Diaz de la Rubia, J. Tarus, Phys. Rev. B 57 (1998) 7556–7570.
[52] A. Stukowski, V.V. Bulatov, A. Arsenlis, Model. Simulat. Mater. Sci. Eng. 20 (2012), 085007.
[53] A. Stukowski, Model. Simulat. Mater. Sci. Eng. 18 (2010), 015012.
[54] A. Stukowski, V.V. Bulatov, A. Arsenlis, Model. Simulat. Mater. Sci. Eng. 20 (2012), 085007.
[55] N. Soneda, S. Ishino, T.D. de la Rubia, Phil. Mag. Lett. 81 (2001) 649–659.
[56] M. Hou, Nucl. Instrum. Meth. 182–183 (1981) 153–162.
[57] D. Terentyev, C. Lagerstedt, P. Olsson, K. Nordlund, J. Wallenius, C. Becquart, L. Malerba, J. Nucl. Mater. 351 (2006) 65–77.
[58] A. Sand, J. Dequeker, C. Becquart, C. Domain, K. Nordlund, J. Nucl. Mater. 470 (2016) 119–127.
[59] F. Granberg, J. Byggmästar, A.E. Sand, K. Nordlund, EPL (Europhysics Letters) 119 (2017) 56003.
[60] M.L. Jenkins, M.A. Kirk, W.J. Phythian, J. Nucl. Mater. 205 (1993) 16.
[61] B.N. Singh, S.J. Zinkle, J. Nucl. Mater. 206 (1993) 212–229.
[62] M. Eldrup, B.N. Singh, J. Nucl. Mater. 323 (2003) 346–353.
[63] K. Nordlund, R.S. Averback, Phys. Rev. B 59 (1999) 20–23.
[64] A. Calder, D. Bacon, A. Barashev, Y. Osetsky, Phil. Mag. 90 (2010) 863–884.
[65] A. Sand, K. Nordlund, S. Dudarev, J. Nucl. Mater. 455 (2014) 207–211.
[66] M.-C. Marinica, F. Willaime, J.-P. Crocombette, Phys. Rev. Lett. 108 (2012), 025501.
[67] R. Alexander, M.-C. Marinica, L. Proville, F. Willaime, K. Arakawa, M.R. Gilbert, S.L. Dudarev, Phys. Rev. B 94 (2016), 024103.
[68] K. Nordlund, M. Ghaly, R.S. Averback, M. Caturla, T. Diaz de la Rubia, J. Tarus, Phys. Rev. B 57 (1998) 7556–7570.
[69] M. Ghaly, K. Nordlund, R.S. Averback, Philos. Mag. A 79 (1999) 795–820.
[70] K. Nordlund, Comput. Mater. Sci. 3 (1995) 448–456.